ETH

Eidgenössische Technische Hochschule Zürich
Swiss Federal Institute of Technology Zurich

SEMESTER THESIS

Superconducting Mach-Zehnder Interferometers for Circuit Quantum Electrodynamics

Laboratory for Solid State Physics
ETH Zürich, Switzerland

Presented by:	Gebhard Littich
Carried out at:	Quantum Device Lab
Supervisors:	Dr. Peter Leek
	Prof. Dr. Andreas Wallraff

Zürich, April 2009

Abstract

In the field of quantum electrodynamics (QED) the interaction between light an matter is investigated. It has recently become possible to access this field by coupling photons in superconducting circuits to artificial two-level atoms (qubits) [1].

In experiments with optical photons, a beam splitter can be used to split a photon into a superposition of two paths and therefore create quantum entanglement. In this semester thesis, the design and measurement of superconducting circuit equivalents to beam splitters and Mach-Zehnder Interferometers are discussed. Building on previous semester theses (see Ref. [2], [3]) existent beam splitter designs were re-fabricated. A set of superconducting Mach-Zehnder Interferometer circuit designs were made, to assess their use in circuit QED experiments, and in particular their application to qubit readout.

The dependence of measured scattering parameters of such circuits on measurement setups was investigated. It was found, that it is crucial to eliminate impedance mismatches in the measurement setup cabling for optimal performance of the experiment. Measurements of beam splitter devices agreed qualitatively with theory and simulations, but better grounding of coplanar circuits is likely to be needed to improve future experiments.

Contents

1 Introduction

In the last two decades, technical advances have allowed physicists to experimentally access the quantum mechanical nature of many physical systems. Many new applications of theoretically well-understood aspects arose from difficulties concerning measurement precision, noise or cooling. In particular, unprecedented levels of control over individual quantum systems has allowed the birth of the field of quantum computing. Still far away from everyday working systems, first experimental efforts have been reported in the fields of superconducting circuits, ion traps, semiconductor quantum dots and NMR. Superconducting circuits provide high scalability and can be fabricated easily using techniques known from conventional integrated circuit fabrication.

Circuit Quantum Electrodynamics

A recent advance in the field of superconducting circuits has shown [1] that it is possible to couple a superconducting two-level system (qubit) to a single photon in a microwave cavity, realized e.g. by a transmission line resonator on a integrated microchip. This system provides a strong interaction between photons and a solid-state system, i.e. light and matter, called circuit quantum electrodynamics. It is of particular interest for quantum computing since many qubits can be coupled together via the resonator.

Beam splitters

A beam splitter classically divides an incident beam of light into two equal paths (see Figure 1.1, a). This is achieved by using a half-silvered mirror as splitting device. It reflects one half and transmits the other half of the incident light intensity. Considering a single photon source, a beam splitter creates a superposition of two paths. It therefore can be observed that it is impossible to detect one photon simultaneously at output port 1 and 2. One could use a beam splitter in circuit QED to entangle qubits in different resonators by sending single photons through.

To encourage such realizations for circuit QED, the equivalent to an optical beam splitter needs to be found. In a previous semester thesis [2] beam splitters were employed in microwave circuits by making use of the design of quadrature hybrids. Quadrature hybrids are a four-port microwave networks exploiting interference effects that allow a symmetric splitting of an incoming signal. Both outgoing signals have the same amplitude and are phase shifted by 90 degrees. Such systems are therefore also called 90 degree quadrature hybrids.
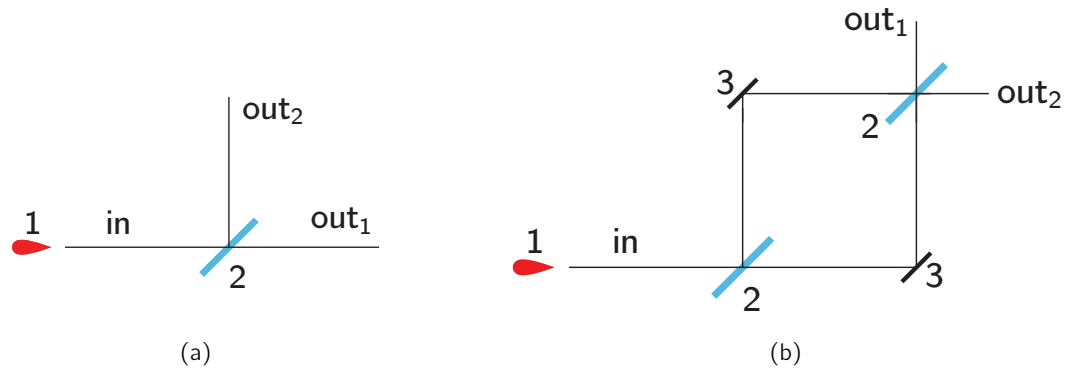
Figure 1.1: a) Sketch of an optical beam splitter. Incident light *in* from a source (1) is divided into *out₁* and *out₂* by a half-silvered mirror (2). b) Sketch of a Mach-Zehnder Interferometer. An incoming beam is being split into two paths (2), transmitted over a mirror (3) and collected by another beam splitter (2). Figures taken from [3].

Mach-Zehnder Interferometers

Incorporating two beam splitters leads to the Mach-Zehnder Inteferometer. Named after physicists Ludwig Mach and Ludwig Zehnder, it used to show phase shifts between two coincident beams (see Figure 1.1, b). One could manipulate one path by e.g. varying its length leading to interference fringes seen on a detector collecting both arms.

Creating a Mach-Zehnder Interferometer in circuit QED by arranging two microwave beam splitters in series on a integrated microchip would allow experiments to be carried out on individual microwave photons. Applying a resonator at one arm of the MZI and coupling a qubit non-resonantly could provide an alternative to current qubit measurements, which may in theory reach the quantum limit [4].

Thesis Outlook

In this thesis I have investigated the reliability of beam splitting devices for circuit QED and continued the work that was begun in [2] and [3].

The first part of this thesis a analysis of beam splitters is presented. I compare ideal characteristics and simulations to measurement results and discuss the attempt to resolve non-idealities of the measurement setup.

The second part mainly focuses on the design process and integration of two beam splitters into a Mach-Zehnder Interferometer. I also characterize the implementation of $\lambda/4$ resonators attached to one arm of a Mach-Zehnder Interferometer and discuss the qualitative effect of a single qubit coupled to the resonator cavity.

2 Beam splitter devices

2.1 Theoretical Introduction

An optical beam splitter, e.g. a half-silvered mirror, does not translate directly into a microwave circuit. One may however construct certain circuits of transmission lines that behave as beam splitters over a certain frequency range. An example of such a circuit is the quadrature hybrid. In order to explain the theoretical principles of these hybrids, I want to explain the main facts about microwave engineering in this chapter.

The characterization of transmission lines besides network analysis techniques play the biggest role in understanding complex circuits. A transmission line is characterized by its length and impedance Z (or often denoted by Z_0). Connecting transmission lines with different impedances leads to reflections at the interface. Mismatches of this kind can significantly effect measurement results, as will be shown later in this chapter.

Network Analysis Basics

A microwave network consisting of complications like T-junctions rather than simple straight transmission lines may not longer be analyzed easily. To work out such a system completely, solving Maxwell's equations at any place at any time would be necessary. By introducing *scattering matrices* (see [5] for more detailed description), these complex calculations can be avoided. A scattering matrix pictures reflections or transmissions happening at the different ports of a circuit. By simplifying a circuit to a system of only two ports, one can derive a transmission (also ABCD-) matrix, that is given by [5]:

$$\begin{pmatrix} V_1 \\ I_1 \end{pmatrix} = \begin{pmatrix} A & B \\ C & D \end{pmatrix} \begin{pmatrix} V_2 \\ I_2 \end{pmatrix},\tag{2.1}$$

where V_1 and V_2 are the voltages, and I_1 and I_2 the different currents at ports one and two.

In order to describe the behavior of a quadrature hybrid, one can divide the circuit shown in 2.1 into the superposition of an even-mode and odd-mode-excitation. The amplitude of the incident even and odd waves at port 1 are given by $1/2$ whereas at port 4 by $\pm 1/2$. The total incident amplitude for port 1 therefore adds up to 1, and for port 4 it adds up to zero, which corresponds with port 1 being our input and port 4 being our terminated port. We can furthermore decompose even- and odd-mode excitations into two decoupled two-port-networks making use of symmetries
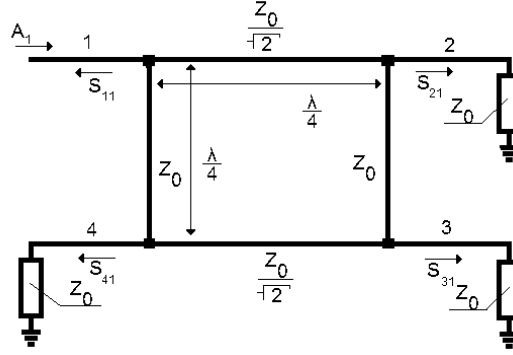
Figure 2.1: Schematic circuit design of a microwave beam splitter (quadrature hybrid). Z_0 denotes the transmission line impedance, $\lambda/4$ its lenght and S_{11}, S_{21}, S_{31}, S_{41} entries of the beam splitter's specific scattering matrix. Transmission lines have the same length, opposite lines have the same impedance each. Figure taken form [2].

and find their specific ABCD-matrices. These are given by (note indices e and o):

$$
\begin{pmatrix} A^{e} & B^{e} \\ C^{e} & D^{e} \end{pmatrix} = \begin{pmatrix} 1 & 0 \\ \frac{i}{Z_0}\tan\left(\beta l_1\right) & 1 \end{pmatrix} \begin{pmatrix} \cos\left(\beta l_2\right) & \frac{iZ_0}{\sqrt{2}}\sin\left(\beta l_2\right) \\ \frac{iZ_0}{\sqrt{2}}\sin\left(\beta l_2\right) & \cos\left(\beta l_2\right) \end{pmatrix} \begin{pmatrix} 1 & 0 \\ \frac{i}{Z_0}\tan\left(\beta l_1\right) & 1 \end{pmatrix} \tag{2.2}
$$

$$
\begin{pmatrix} A^{o} & B^{o} \\ C^{o} & D^{o} \end{pmatrix} = \begin{pmatrix} 1 & 0 \\ \frac{-i}{Z_0}\tan\left(\beta l_1\right) & 1 \end{pmatrix} \begin{pmatrix} \cos\left(\beta l_2\right) & \frac{iZ_0}{\sqrt{2}}\sin\left(\beta l_2\right) \\ \frac{iZ_0}{\sqrt{2}}\sin\left(\beta l_2\right) & \cos\left(\beta l_2\right) \end{pmatrix} \begin{pmatrix} 1 & 0 \\ \frac{-i}{Z_0}\tan\left(\beta l_1\right) & 1 \end{pmatrix} \tag{2.3}
$$

The wave dispersion relation β is given by $\beta = \frac{2\pi f}{c/\sqrt{\epsilon}}$, ϵ denotes the dielectric constant of the substrate. l_1 and l_2 refers to the length of the subcircuit elements the network was intersected in. Due to our specific lengths, we get $l_1 = \lambda/8$ and $l_2 = \lambda/4$.

Because the measurement device records elements of the scattering matrix, we want to recalculate them by making use of following equations. Since the system is linear, the total excitation is given by the sum of the even- and odd-mode excitations, i.e. the scattering matrix elements introduced in equations 2.2 and 2.3.

$$
S_{11} = \frac{1}{2}S_{11}^{e} + \frac{1}{2}S_{11}^{o}, \tag{2.4}
$$

$$
S_{21} = \frac{1}{2}S_{21}^{e} + \frac{1}{2}S_{21}^{o}, \tag{2.5}
$$

$$
S_{31} = \frac{1}{2}S_{21}^{e} - \frac{1}{2}S_{21}^{o}, \tag{2.6}
$$

$$
S_{41} = \frac{1}{2}S_{11}^{e} - \frac{1}{2}S_{11}^{o}, \tag{2.7}
$$

where $S_{11}^{e,o}$ and $S_{21}^{e,o}$ is given by:

$$
S_{11}^{e,o} = \frac{A^{e,o} + B^{e,o}/Z_0 - C^{e,o}Z_0 - D^{e,o}}{A^{e,o} + B^{e,o}/Z_0 + C^{e,o}Z_0 + D^{e,o}}, \tag{2.8}
$$

$$
S_{21}^{e,o} = \frac{2}{A^{e,o} + B^{e,o}/Z_0 + C^{e,o}Z_0 - D^{e,o}}. \tag{2.9}
$$

To give a better view of this ideal behavior of the beam splitter, the S-parameters can be plotted sweeping the frequency on the x-axis (see figure 2.2).
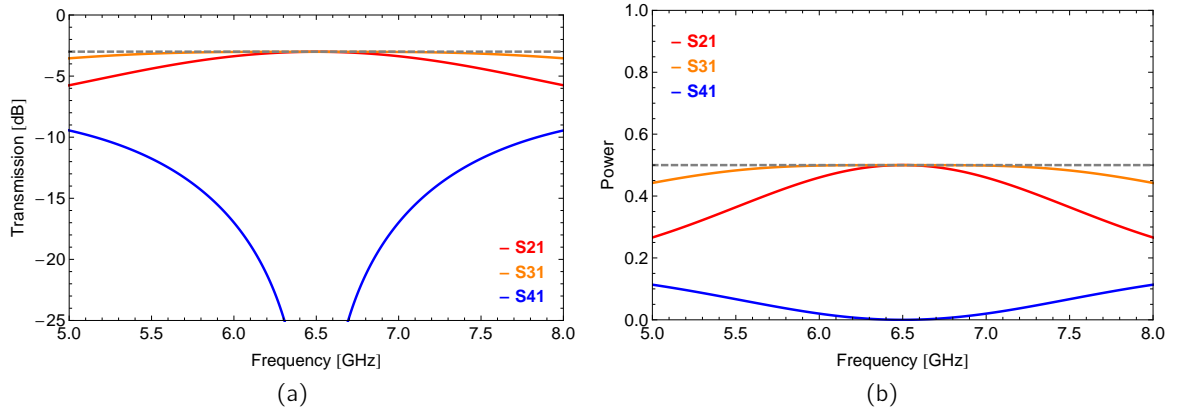

(a)

(b)

Figure 2.2: a) S-parameters of a single beam splitting device, working at a frequency of 6.5 Ghz. In a range about this frequency, the beam splitter works ideally in a optimal way and divides the incoming microwave into two equal signals of transmission 3 dB each (see gray dashed line). Port 4 in our notation refers to the terminated port and so no signal should be transmitted there. This corresponds to a centered dip. b) Same plot with linear scaling.

Coplanar Waveguide implementation

After characterizing the beam splitter model theoretically, it was necessary to think about actual implementations for microwave circuits. In [2], comments on microstrip and coplanar waveguide technology were made. Due to fabrication and size reduction issues it became obvious to use coplanar waveguides (abbr. CPW) as transmission lines for our circuits. In figure 2.3 you can see a cross-section of a typical coplanar waveguide. Impedances are dependent on the waveguide's dimensions a/b and can therefore be scaled easily. More precisely, conductor-backed CPW were chosen.

Calculating impedances can be carried out by either using software *TXLine*. Or, although not taking into account the substrate thickness t, by solving following expression analytically [6]:

$$Z_0 = \frac{60\pi}{\sqrt{\epsilon_{\text{eff}}}} \frac{1}{\frac{K(k)}{K(k')} + \frac{K(k_3)}{K(k_3')}}, \tag{2.10}$$

where the complete elliptic integral of first order $K(k)$ is given by

$$K(\alpha) = \int_0^{\pi/2} \frac{d\theta}{\sqrt{1 - \alpha^2 \sin^2(\theta)}}, \tag{2.11}$$

and

$$k = a/b, k_3 = \frac{\tanh(\pi a/2h)}{\tanh(\pi b/2h)}, k' = \sqrt{1 - k^2}, k_3' = \sqrt{1 - k_3^2}. \tag{2.12}$$

The effective dielectric constant ϵ_{eff} is a function of the relative permittivity ϵ_{r} of the dielectric
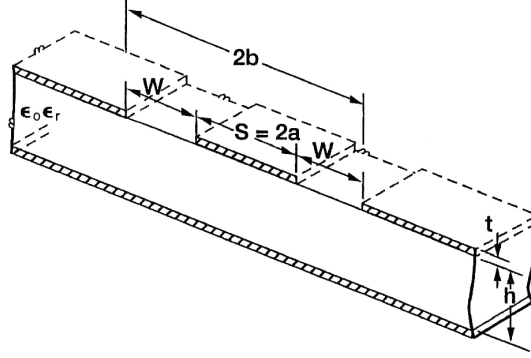
Figure 2.3: Cross-section of a conductor backed CPW. This model consists of a center conductor of width $S = 2a$ faced by two ground planes with a distance W. The line's impedance is dependent of the ratio a/b. In this sketch h corresponds to the height of the dielectric ground plane, and t to the thickness of the conducting substrate, in our case Niobium. Figure taken from [6].

substrate and the geometry of the waveguide:

$$\epsilon_{\text{eff}} = \frac{1 + \epsilon_{\text{r}} \frac{K(k')}{K(k)} \frac{K(k_3)}{K(k_3')}}{1 + \frac{K(k')}{K(k)} \frac{K(k_3)}{K(k_3')}}. \tag{2.13}$$

To calculate the lengths of the CPW lines, we have to bear in mind that the electrical lengths must correspond to $\lambda/4$ or 90 degrees, as can be seen in figure 2.1. To obtain the effective length needed in our model, we use:

$$L = \frac{L_{\text{EL}} c}{360 \sqrt{\epsilon_{\text{eff}}} f_{\text{d}}}, \tag{2.14}$$

where L_{EL} is the electrical length given in degrees, c speed of light, ϵ_{eff} the effective dielectric constant and f_{d} the design frequency. It follows, that the design frequency the optimal beam splitter should work at is constrained to the length of the lines only.

Beam splitter design and fabrication

After figuring out appropriate dimensions for the CPW, a design for the beam splitting device had to be found, see figure 2.4. As this was mainly done in [2], I will not explain this process in detail and only consider modifications, I carried out. To gain more flexibility with respect to modifying crucial parameters like CPW dimensions on demand, I redrew the whole design in Mathematica. For the realization in the Mach-Zehnder-Inteferometer, I rotated the device by 90 degrees to fulfill the condition of terminated port 4 lying at the top besides incoming port 1.

In order to fabricate the devices, we ordered a quartz glass mask. I then, together with Gabriel Puebla and Lars Steffen, created the beam splitter structures on a niobium-coated sapphire wafer with standard photolithographical methods.

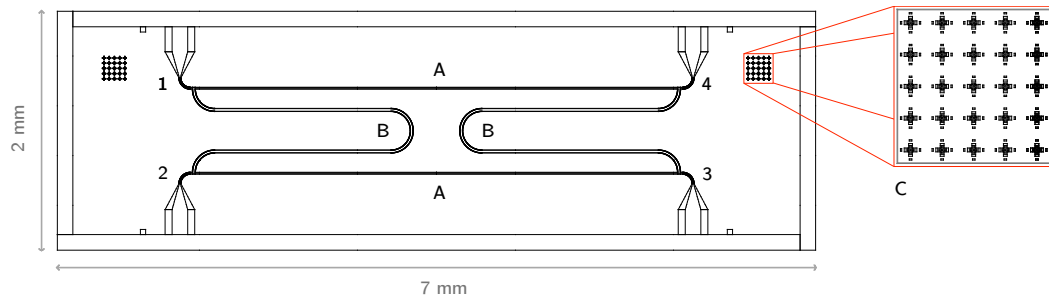To prevent excitations of unwanted coupled slot line modes of the circuit, microwave engineers

Figure 2.4: 6.5 GHz coplanar waveguide design of a beam splitting device (labelled Z1/Z2). (1) to (4) denote the port numeration. Niobium CPW lines each have a length of $4670\,\mu m$: lines (A) correspond to an impedance of $Z_0 = 50\,\Omega$ whereas lines (B) correspond to $Z_0/\sqrt{2} = 35.35\,\Omega$. CPW dimension are given by $a_1 = 5.0\,\mu m$ and $b_1 = 9.5\,\mu m$ for $Z_0 = 50\,\Omega$ and $a_2 = 12.0\,\mu m$ and $b_2 = 15.0\,\mu m$ for $Z_0/\sqrt{2} = 35.35\,\Omega$. In (C) alignment markers for later multi-layer photolitography, e.g. *air-bridges*, are illustrated.
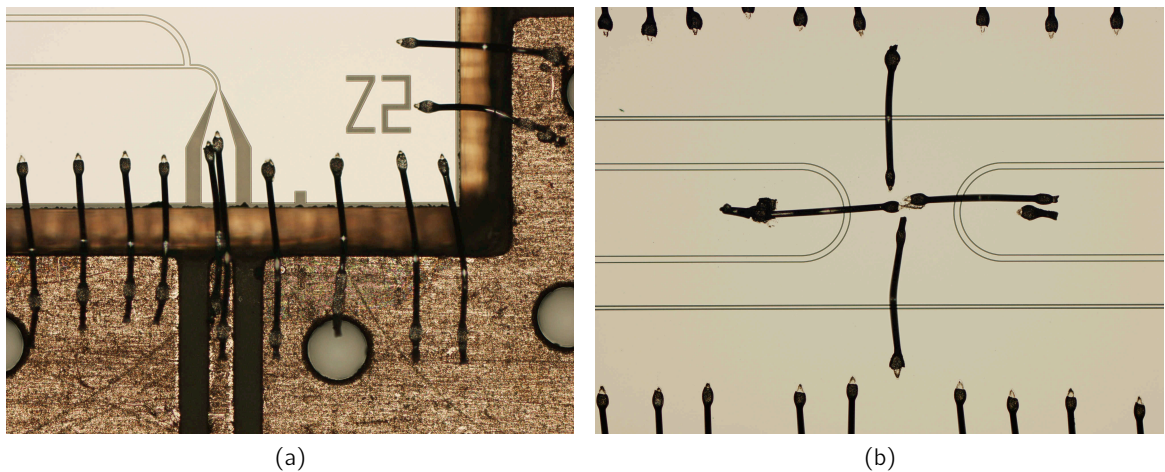

| (a) | (b) |

Figure 2.5: Optical microscope photographs of the beam splitter. a) Aluminum bond wires connecting the PCB (dark) and the chip (bright). b) Over certain positions of the transmission line, bond wires are being attached to keep the electric potential of the ground terminated.

often use air-bridges to keep the ground plane of the coplanar wave guide at zero potential everywhere. These are made of metal (e.g. aluminum) forming a bridge over the center strip conductor connecting opposite sides of the ground plane. They can be applied in a second photolitographical step. As multilayer photolitography needs markers for the alignment of the later masks, I added alignment markers, as seen in the zoomed window in figure 2.4.

As the application of air-bridges can be quite complex and time consuming, one can use bond wires instead. Ideally behaving like air-bridges they can be attached over crucial parts of the transmission lines, e.g. as shown in figure 2.5 b). As will be discussed later on, bond wires do not replace air-bridges satisfactorily.
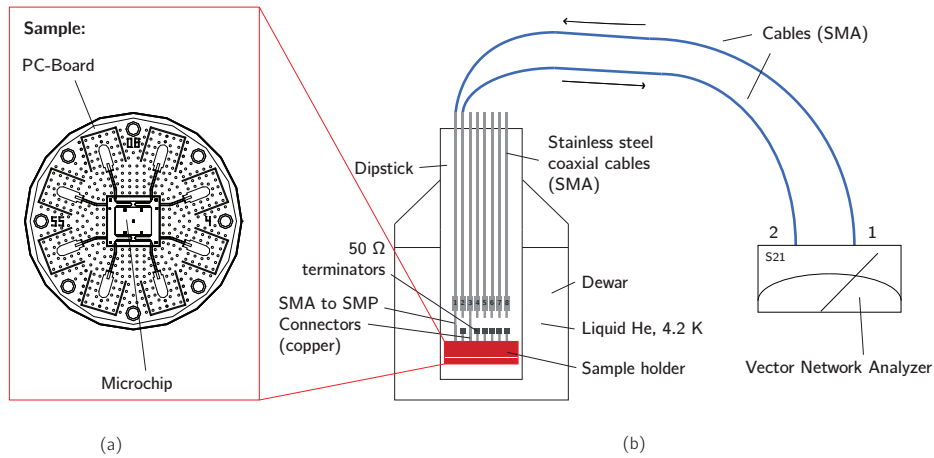
Figure 2.6: Dipstick setup: a) The photolitographically fabricated microchip is glued on a printed circuit board. Then the chip's ground plane and the CPW transmission lines are bond-wired on the board. In this figure a triple-sized chip containing a Mach-Zehnder-Interferometer (see chapter 3) is depicted. b) Sketch of measurement setup with dipstick. *1* at the dipstick is denoted the input port whereas *2* is the output port. The notation *S21* means sending the microwave signal from the VNA into port 1 and analyzing the outcome from port 2. The original dipstick setup has ben modified that unused ports are being terminated directly after the sample holder rather than at the top of the dipstick after the stainless steel cables. This was done to prevent unwanted reflections, as discussed later.

2.2 Measurements

In order to characterize the behavior of the beam splitters they have to be cooled down into the superconducting regime, e.g. in liquid helium. This requires the usage of measurement equipment that is designed for these low temperatures.

2.2.1 Experimental setup

After a design has been fabricated on a microchip, one needs to connect the on-chip super-conducting transmission lines to cables linked to a measuring device. This is accomplished by mounting the microchip on a printed circuit board (PCB) and attaching bond wires between the chip and the board, see figure 2.6 a) and 2.5 a). Finally connector pins have to be soldered on the PCB gaining access via external coaxial cables. The mounting procedure has to be carried out very accurately to avoid unwanted reflections in the later measurement.

Cooling the sample

To measure the circuits in the superconducting regime, the sample then needs to be cooled down below the material's critical temperature T_c. As $T_c = 9.5\,K$ for Niobium, it is sufficient to dip the sample into liquid helium with a temperature of $T = 4.2\,K$. To do so, the PCB

is mounted on a probe holder allowing access to the sample via eight microwave connectors. These connectors are connected via one meter long stainless steel microwave cables to room temperature. This tool is called a dipstick, see figure 2.6 b). It can be clamped at the neck of a dewar and lowered into the liquid by releasing an O-ring clamp. To inhibit extensive evaporation, the dipstick has to be dropped very carefully and slowly. When the system has stabilized into thermal equilibrium, which can be controlled via a gas escape valve, the sample has successfully been cooled down and one can proceed with measuring S-parameters and comparing them to theoretical predictions by using an appropriate measuring device.

Scattering Matrix Measurements

In order to measure entries of the scattering matrix, our instrument of choice is the Vector Network Analyzer (short VNA). With this two-port instrument we are able to determine the elements of this matrix (i.e. S-parameters) by sending microwave signals into a network and measuring their transmission. Sweeping over a certain frequency range leads to different transmission values depending on the emitted frequency. To gather data on a PC, the VNA can be connected via GPIB and read out remotely in a LabView interface. By default the VNA measures the transmission signal in dB, i.e. it is being plotted logarithmically. To scale the transmission plot linearly, following conversion must be done:

$$\frac{P_\text{out}}{P_\text{in}}(\text{L}) = 10^{\frac{\text{L}}{10}},\tag{2.15}$$

where P_out and P_in respectively are the outcoming and incoming power and L is the transmission signal in dB.

After gathering the data (as *.txt-files) from the VNA, it was formatted and plotted in Mathematica.

Setup Calibration

Before actually starting to measure, a calibration was necessary. To avoid deviations of the signal due to losses in the two SMA cables connecting the Vector Network Analyzer and the dipstick, they were shorted via a female-to-female adapter and a two-port through calibration was done. The calibration was performed from 5 to 10 GHz to cover the whole range necessary for the later beam splitter measurements. The dipstick also had to be calibrated, taking losses at the long stainless steel cables inside the rod into account. To achieve this, a PCB-through connecting the used ports 3 and 1 was cooled down inside the dipstick and the transmission was recorded. Later on this was used to evaluate beam splitter data in Mathematica and substract the beam splitter's transmission by the dipstick loss.
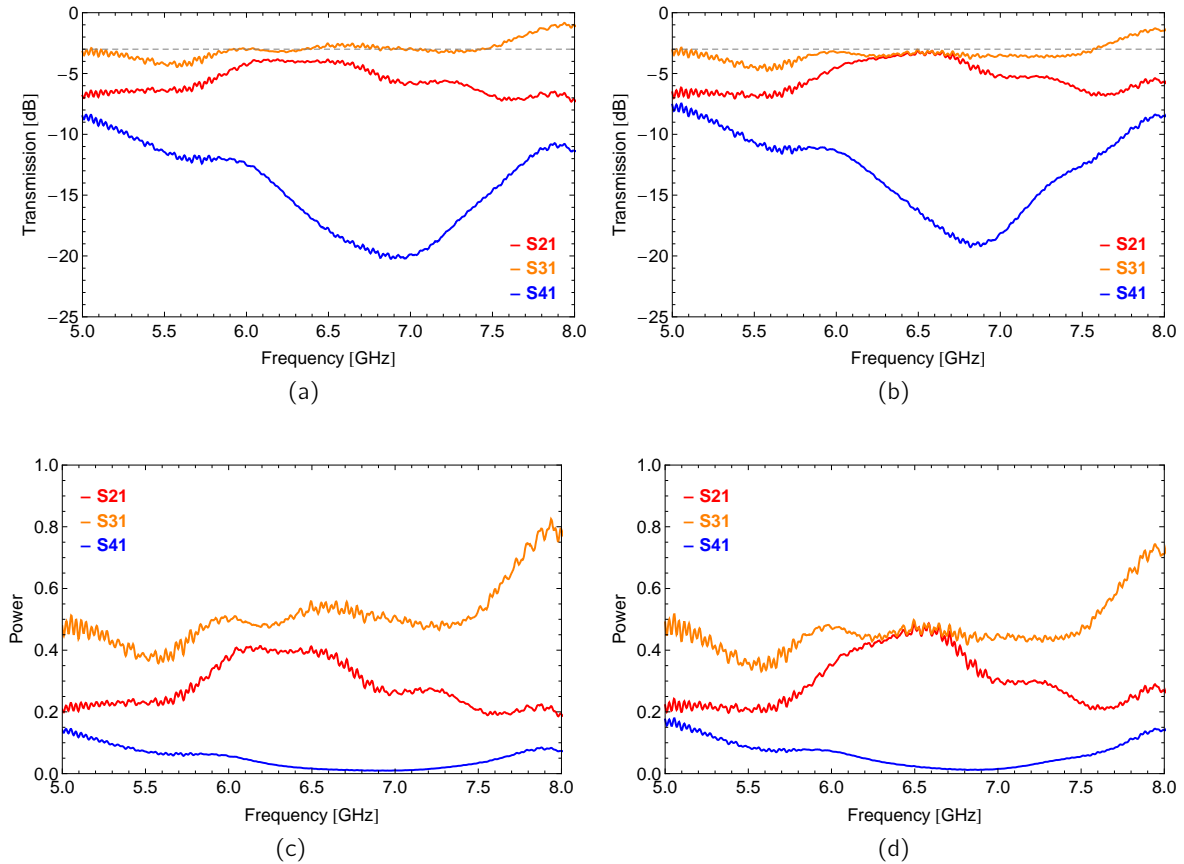
Figure 2.7: Measured transmissions of the beam splitting devices Z1 and Z2 at a working frequency of 6.5 GHz. a) Z1, b) Z2, c) Z1 with a linear scaling, d) Z2 with a linear scaling.

2.2.2 Results

In figure 2.4 I presented the main beam splitting device used in my experiment. We fabricated two copies of this device and labelled it by Z1 and Z2. This device is intended to work at a frequency at about 6.5 GHz, as figure 2.2 also shows. As Z1 and Z2 are de facto the same devices, they should behave in the exact or at least in a very similar way. Inconsistencies could emerge from problems in attaching the chips to the PCB or from differences in the quality of soldering the connecting pins onto the PCB. Such deviations should stay very low, though.

In figure 2.7 the main results are presented. I recorded the transmission parameters S21, S31 and S41 (i.e. entries of the scattering matrix) for both devices and plotted it on a logarithmic and linear scale. With a linear scaling rather than logarithmic it is easier to see if the device works in a symmetric way and both signals are equally split at 50 percent of input transmission. Figure 2.7 a) and c) shows the data of device Z1 and b) and d) of Z2. At first sight both devices seem to work very similarly. Although it is peculiar that the terminated line (S41) dip has not the same low transmission as in theory and there is a deviation of the splitting strength of both devices. Z2 splits the incoming signal quite equally at a frequency of about 6.5 GHz (b), whereas
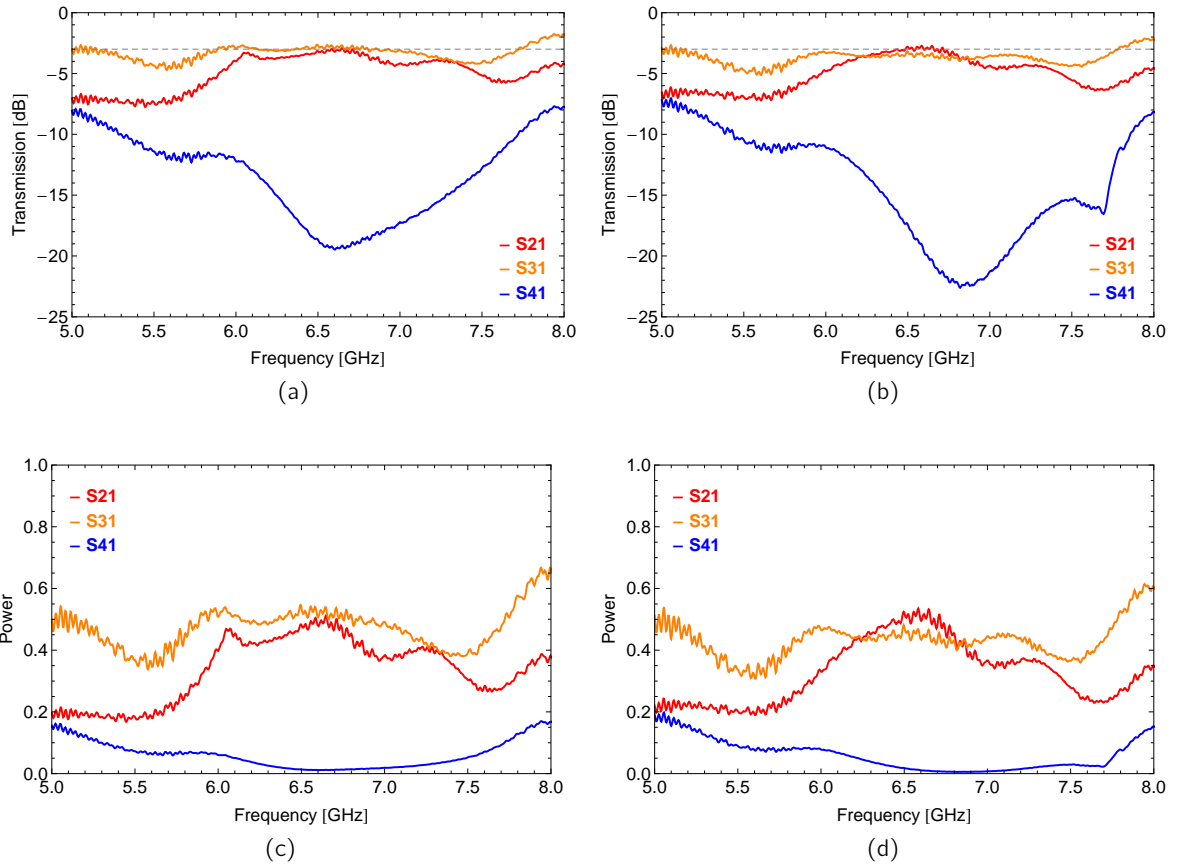
Figure 2.8: Measured beam splitter devices after adding additional bonding wires. a) Z1, b) Z2, c) Z1 linear, d) Z2 linear.

for Z1 S21 and S31 are shifted by about 1.5 dB (a). In [3] similar deviations were encountered. This shift cannot be explained by inaccuracies of the fabrication or miscalculations of specific geometries like line length or gap distances. It is rather possible, that the electrical ground of the coplanar wave guide is not terminated sufficiently, causing unwanted mode excitations.

Additional bond wires

As it already has been shown in [3], there is an effect of putting bond wires over crucial parts of the chips in order to keep the electric potential terminated. I wanted to determine the impact of placing even more bonding wires on the fidelity of the chip. We therefore put some bonds over the T-junctions of the beam splitter (see figure 2.9) and measured the transmission afterwards. Figure 2.8 shows the corresponding data. Though the deviation between S21 and S31 in 2.9 a) has reduced, it must be noticed that the good agreement to theory of 2.7 b) is only coincidental. The similarity in the results in figure 2.8 and 2.7 indicates that the advantage does not seem to be essential, though.

Sonnet 3D-EM-simulations have shown, that the thickness of the bonding wires in the center of

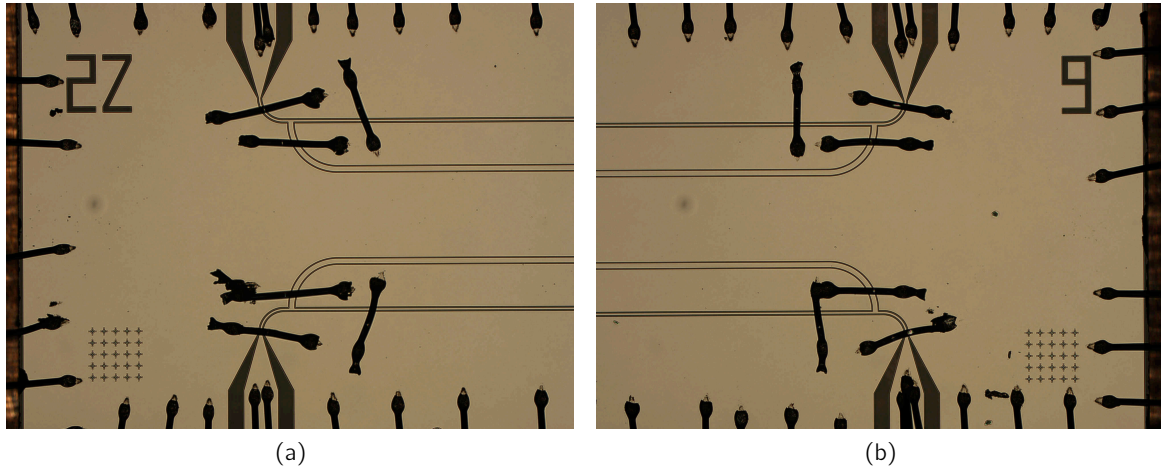(a)   (b)

Figure 2.9: Optical microscope photographs after additional bond wires were attached over the beam splitter's T-junctions (here device Z2).

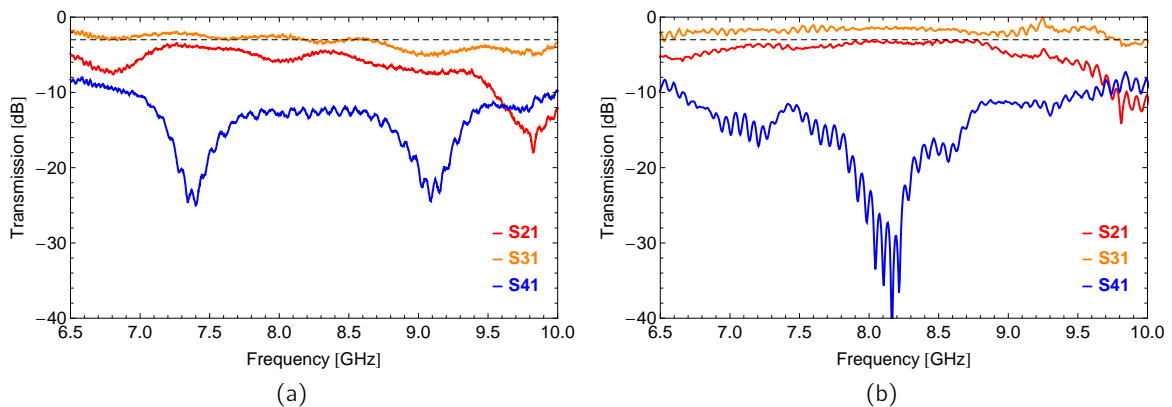(a)   (b)

Figure 2.10: a) Measurement of device T5 with a work frequency of 8.29 GHz. b) Henzen's measurement of the same device.

the chip (figure 2.5 b)) could play a role. Applying more- or thicker bond wires could therefore reduce the deviations by slowly approaching the characteristics of an ideal air-bridges. Therefore it is highly likely that only real air-bridges at the T-junctions and over the center bends significantly effect the behavior and will therefore be required for highly reliable systems.

2.2.3 Experimental issues

Before measuring the data presented above, I had considerable problems finding a confident measurement setup. When Henzen in [3] measured his samples, he worked with an older version of the dipstick only providing four measuring ports. In his dipstick the long coaxial cables were also not made of steel but copper. He used to connect all ports with the long coaxial cables and terminate unused ports at the top of the dipstick (at room temperature) with a $50\,\Omega$ terminator. When I tried to do my first measurements, I did the the same with the new configuration
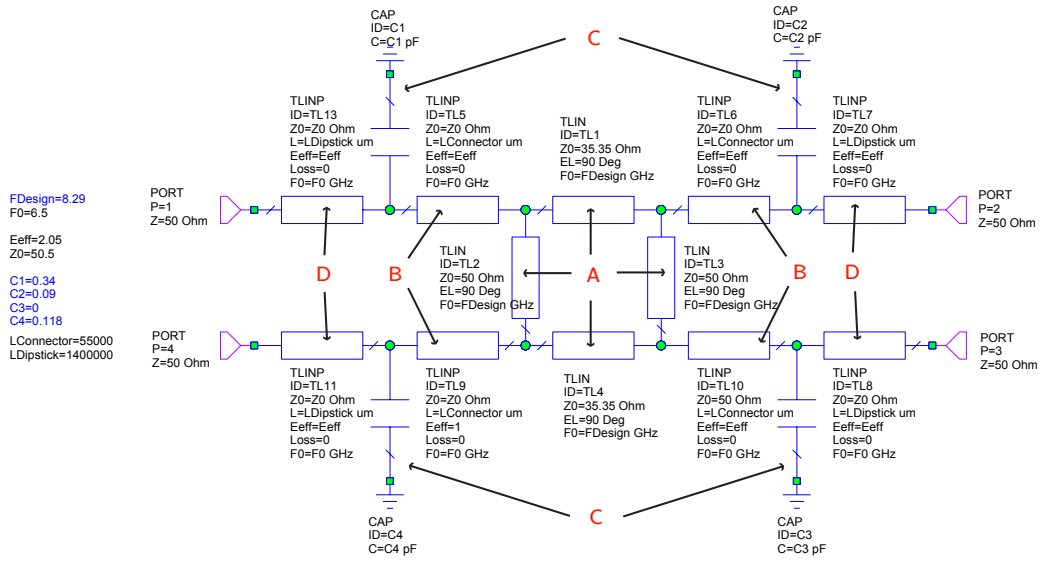
Figure 2.11: Microwave office schematic for simulation of beam splitter measurement inside the new dipstick. (A): Beam splitter, (B): short copper cables with length of 5.5 cm, (C): Capacitances simulating reflections at SMA-SMP connectors in picofarad range, (D): long stainless steel coaxial cables with length of 140 cm.
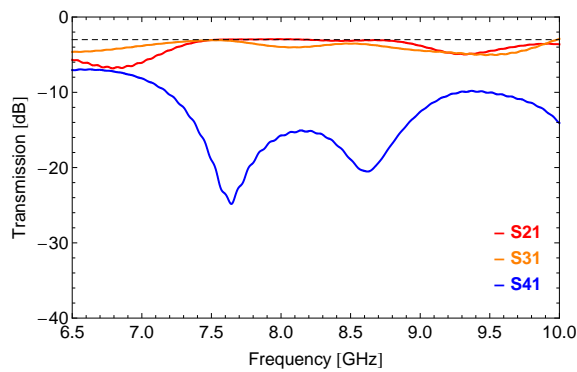

Figure 2.12: MWO simulation for schematic in figure 2.11.

providing 8 ports. To become familiar with the experiment, I took an old sample, *T5* with a working frequency of 8.29 GHz, that Henzen had already measured before. I experienced results that were differing from his results strongly. Figure 2.10 a) shows that the dip at the working frequency is split in two independent features with higher transmission, and oscillations deviate the splitting lines $S21$ and $S31$.

Microwave Office

To find the cause for these issues, I then set up a *Microwave Office* simulation for the beam splitting circuit. To simulate the behavior of the dipstick, I incorporated all connecting cables and fitted them with appropriate parameters for length, impedance and frequency. In figure 2.11 the corresponding schematic is shown. The additional capacitances being ground at the cable

connections (see figure 2.12, (C)) simulate reflections arising from impedance mismatches in the SMA-SMP copper connectors. As you can see in figure 2.12, I was able to reconstruct the main features and dips at 7.5 and 9 GHz qualitatively quite well. With Microwave Office it is not possible to perform a full 3D-EM simulation, though, and therefore the problem of a bad termination of the ground was not taken into account. This explains why I could not simulate the unequal splitting adequately.

Final setup

Due to these problems we thought about the measurement setup carefully and tried to improve the results by changing the dipstick configuration. After going back to the older 4-port dipstick and trying to use different short connectors, we came to the conclusion that the dipstick should work in the best way when the unused ports are terminated directly after the probe holder instead at the top of the dipstick. Doing that we could at least avoid reflections coming from the long steel cables. From this change another experimental issue became obvious. Terminating in cold regime involves the necessity of heating the sample up and cooling it down again after each measurement. This made the experiment more time consuming. However, the changes of the setup significantly improved the measurement results, which matched better with theory, as can be seen in fig. 2.7.

3 Mach-Zehnder-Interferometer devices

In classical optics Mach-Zehnder Interferometers (MZI) are usually built of two optical beam splitters (e.g. half silvered mirrors) and two totally reflecting mirrors, see figure 3.1 a). By varying the path between the beam splitters, one can then see interference fringes on a screen (detector). One application of this device may arise for a fast and easy qualitative analysis of unknown samples, e.g. crystal structures. As the phase of the beam directed through the sample will be altered, one can then observe material-specific interference effects at the detector screen.

For applications with superconducting circuits one can build MZIs by incorporating two microwave beam splitters introduced in chapter 2. As the understanding of superconducting MZIs requires prior knowledge of the simpler optical case, I want to give a short theoretical introduction.

3.1 Theory

As the theory of optical beam splitters and interferometers also holds for microwave circuits, one can easily describe the behavior of a Mach-Zehnder-Interferometer built of microwave beam splitters.

3.1.1 Optical Interference

The absolute intensity of the inference term (responsible for observation of interference fringes) of two waves is proportional to the cosine of their phase difference, i.e [7]:

$$|I| \propto |\cos(\delta)|, \tag{3.1}$$

with δ being the phase difference. 90 degree quadrature-hybrids split an incident wave into two waves, one being shifted by 90 degrees in phase. Considering that the signal at two opposite ports 3 and 4 (see figure 3.4) of the microwave Mach-Zehnder Interferometer are therefore shifted by 90 degrees, one can write for the intensities:

$$|I_3| \propto |\cos(\delta)|, \tag{3.2}$$
$$|I_4| \propto |\cos(\delta + \pi/2)| = |\sin(\delta)|. \tag{3.3}$$

As the absolute values of the intensities are proportional to the scattering parameters, e.g. $S21$, we can directly explain figure 3.1, a Microwave Office simulation plot of a MZI with a tunable phase shift in one arm. Although we are sweeping over the phase shift from zero to π in figure
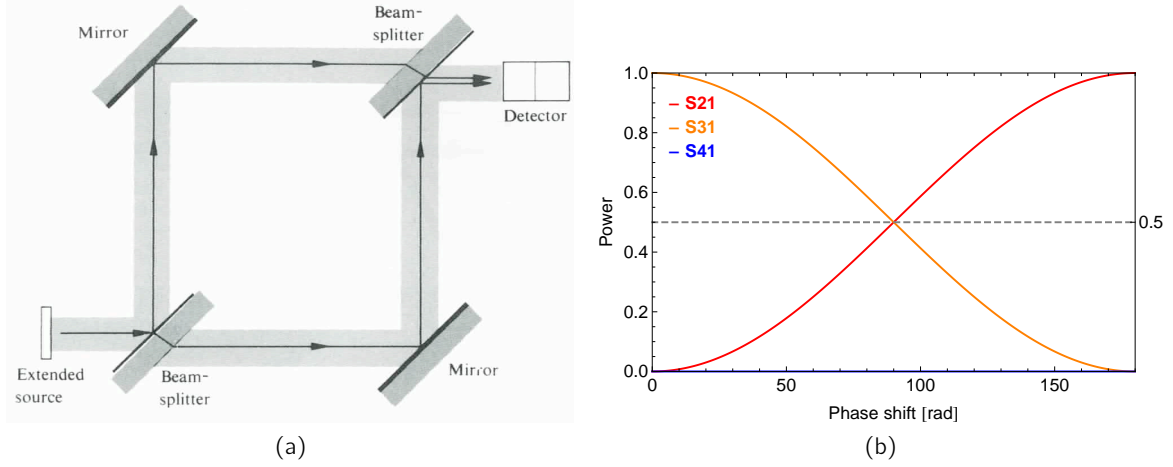
(a) (b)

Figure 3.1: a) Sketch of an optical Mach-Zehnder Interferometer consisting of two half-silvered mirrors working as beam splitters. Figure taken from [7]. b) Power shifting at output ports sweeping over a phase shift, while the input frequency is kept constantly at 6.5 GHz. At zero, it corresponds to fig. 3.1, i.e. a straight through whereas at $\pi/2$ it corresponds to a 90 degree phase shift as in 3.4 a) (B) and at π to a 180 degree shift as in 3.4 a) (C).

3.1, we only fabricated devices corresponding to a discrete shifts of π and $\pi/2$ as well as a straight through with zero shift.

3.1.2 $\lambda/4$ Resonators and Qubit coupling

In order to understand the behavior of coplanar waveguide resonators applied to a MZI circuit (see section 3.2), I want to give a short overview about basic resonator properties. A resonator is basically formed of a CPW transmission line where the center conductor is coupled to an input signal by a capacitor realized by either gap capacitors (for small coupling with capacities in the range of 0.1 fF) or finger capacitors (to achieve a larger coupling, in the range of 10 fF). Also see [8] for a detailed discussion.

Coupling a qubit to a resonator

In circuit quantum electrodynamics, it has been shown (see [9]) that it is possible to couple a qubit dispersively to a microwave cavity, i.e. a resonator. In this dispersive limit, i.e. $|\Delta| = |\omega_a - \omega_r| \gg g$, with ω_a the atomic transistion frequency, ω_r the resonance frequency of the cavity, and g the coupling constant, the Jaynes-Cummings Hamiltonian H (e.g. see [1]), modelling the cavity QED system diagonalizes approximately to:

$$H \approx \hbar \left(\omega_r + \frac{g^2}{\Delta} \right) a^\dagger a + \frac{1}{2} \hbar \left(\omega_a + \frac{g^2}{\Delta} \right) \sigma_z, \tag{3.4}$$

with $a^\dagger a$ the number operator describing the photons in the cavity and $\sigma_z = (|e\rangle \langle e| - |g\rangle \langle g|)$. States $|e\rangle$ and $|g\rangle$ describe the excited- and ground state of the two-level qubit. When a qubit
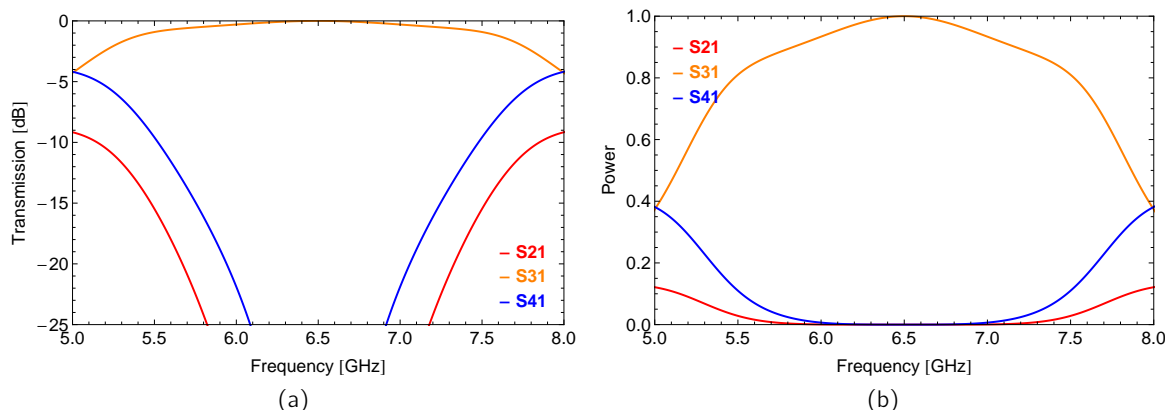
Figure 3.2: a) Microwave Office Simulation of straight through MZI (device A1, also see figure 3.4 (A)). This plot corresponds to a zero phase shift, i.e. both arms having the same length as in fig. 3.2 at zero. a) measured in dB. b) Same plot in linear scaling.

is coupled to the resonator, there is a qubit-state dependent shift of the resonance frequency (see figure 3.3). As the transmission changes when the qubit in the excited state $|e\rangle$, one could now measure the S-parameters at fixed frequency (e.g. at the resonance frequency of the resonator without a qubit) to determine the state of the qubit. The use of an MZI for qubit experiments has been discussed in length in appendix H of [4]. There, it is shown however that it is only possible to reach the quantum limit with an Fock state input. For coherent states the quantum limit can only be reached with an unbalanced second beam splitter, whereas for symmetric devices the quantum limit would be missed by a factor of two.

Alternative qubit coupling options

Instead of coupling the qubit to a $\lambda/4$ resonator, one could also couple it to a $\lambda/2$ resonator or directly to a transmission line of one arm (see figure 3.4 a) K and b) D). The first option requires, however, the resonator being in resonance with the input. With an off-resonant resonator no transmission would get through the MZI. The second option needs a very strong qubit coupling to the transmission line to cause significant phase shifts, but on the other hand a weak coupling to maintain good qubit coherence. Thus, both options seem rather disadvantageous.

3.2 Designs

In order to fit two beam splitters on one chip and keep the opportunity to put transmission lines of half the wavelength in minimum in between, we had to make use of a triple-sized chip. It has three times the height of the chip introduced in figure 2.4, i.e $7000\,\mu m$ in width an $6000\,\mu m$ in height. After choosing appropriate dimensions for the chip and thinking about the best way to fit both beam splitters onto it I began to incorporate the Mathematica designs I had already created before (see chapter 2). I placed both splitters at the very top and bottom of the chip,
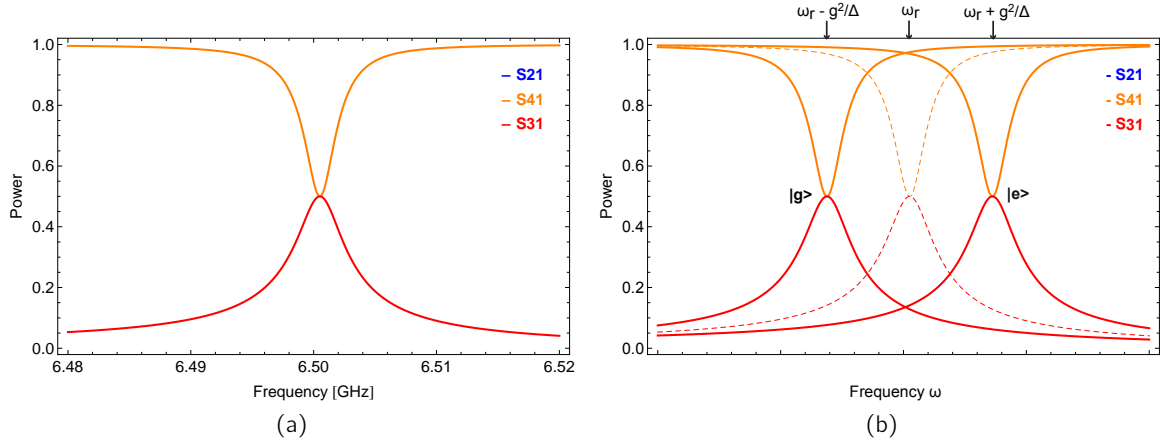
Figure 3.3: a) Microwave Office simulation of a $\lambda/4$ resonator coupled to one arm of a MZI by a 14.8 fF capacitor (e.g. devices G and H, also see table 3.1 and fig. 3.4 b)). The resonator's frequency has been tuned to 6.628 GHz. b) Qualitative behavior when a qubit is coupled to the resonator dispersively: The resonator frequency is shifted down for the qubit being in the ground state $|g\rangle$ and up for the excited state $|e\rangle$. The frequency difference between $|e\rangle$ and $|g\rangle$ is given by $\Delta\omega = 2g^2/\Delta$ with g the coupling constant and detuning $\Delta = \omega_a - \omega_r$ as introduced before.

providing enough space for various manipulations to the arms of the MZI.

3.2.1 Samples

Straight through and phase shift MZI

To characterize the general behavior of a circuit MZI, I connected both beam splitter via a straight transmission line (see figure 3.4 a) (A)). I could also realize a phase shift of 90 and 180 degrees by adding a length of $\lambda/4 = 4670\,\mu m$ and $\lambda/2 = 9340\,\mu m$ to the right arm (see fig. 3.2 and 3.4 a) (B) and (C)).

$\lambda/4$ Resonators

We then thought about implementing $\lambda/4$ resonators into one arm of the Mach–Zehnder Interferometer and creating the possibility for a later Qubit coupling by adding Transmon-gaps besides the resonator transmission line. For each $\lambda/4$ resonator device with transmon gaps I made a copy with an additional charge line going to the qubit to create the possibility to drive the qubit externally.

In order to find the appropriate resonator frequencies f, I simulated the MZI device with Microwave Office and varied the $\lambda/4$-resonator's frequency to tune the resonance of the signals at ports 3 and 4 to the work frequency of the beam splitter devices (lying at 6.5 GHz). Figure 3.3 a) shows a simulation of a resonator tuned to this optimal frequency. Increasing the resonator's frequency would shift the features to the right, decreasing it to the left.

As I made models with different resonator capacitances, I had to repeat this step for each capacitance (25, 14.8 and 4.8 fF) separately. Having the optimal frequency determined, I could calculate the required resonator line length L_{res} by using following conversion:

$$L_{\text{res}} = \frac{2 \cdot L_{\text{c}}}{f}.$$
(3.5)

$L_{\text{c}} = 30530\,\mu m$ is the optimal resonator line length for a $\lambda/2$ resonator, which arose from earlier calculations considering experimental corrections.

3.2.2 Design Process with Mathematica

To draw the MZI devices in Mathematica that were implemented in a Mathematica package before. To e.g. draw a bent line, I just had to call a function delivering the total length and bending radius as parameters. It was important to keep the bending radius of the lines over a minimum of $100\,\mu m$ to avoid unwanted mode excitations.

This made the design process quite easy. Using inversion symmetries I could also mirror basic elements and assemble them to a whole device. Even though Mathematica establishes a neat way of using pre-built functions and manipulating crucial properties like gap distances of the CPW of a whole bunch of devices in a row, I was not always confident about the program's abilities. I e.g. had troubles finding the right coordinates for positioning the circuit elements. Mathematica also works very slowly and memory consuming when a device is being displayed in the notebook.

Wafer layout and mask design

In order to fabricate the devices, the designs needed to be incorporated into an optical mask for photolithography. To put all devices together to a wafer layout, I made use of one of the Mathematica functions again. With them I only had to put the variable names of the devices I wanted to use together in a list. The program automatically arranged the devices in a way they fit best on the wafer. I then exported the complete wafer-layout to the Auto-CAD readable DXF-format to append additional structures like title, date and test structures to the wafer. As a final step, the file had to be converted to GDSII to make it compatible for the company fabricating quartz glass masks.

In table 3.1 you can see an overview of the devices contained on my wafer. For some models we put several copies onto the wafer to make sure to have enough copies for later problems maybe arising. After fabrication, the wafer was diced and the chips were placed on the PCBs (as already described in section 2.2.1).

Label	Type	Device	Res. freq.	Res. cap.	Charge line	Size
A1 - A3	MZI	Straight through	-	-	-	3
B1, B2	MZI	90 degree phase shift	-	-	-	3
C1, C2	MZI	180 degree phase shift	-	-	-	3
D1, D2	MZI	Single Qubit through	-	-	yes	3
E1 - E3	MZI	$\lambda/4$ Res. (6 fingers)	6.718 GHz	25 fF	yes	3
F1, F2	MZI	$\lambda/4$ Res. (6 fingers)	6.718 GHz	25 fF	no	3
G1 - G3	MZI	$\lambda/4$ Res. (4 fingers)	6.628 GHz	14.8 fF	yes	3
H1, H2	MZI	$\lambda/4$ Res. (4 fingers)	6.628 GHz	14.8 fF	no	3
I1 - I3	MZI	$\lambda/4$ Res. (2 fingers)	6.541 GHz	4.8 fF	yes	3
J1, J2	MZI	$\lambda/4$ Res. (2 fingers)	6.541 GHz	4.8 fF	no	3
K1, K2	MZI	$\lambda/2$ High-Q Res.	-	0.93 fF	-	3
Z1 - Z6	BS	Single beam splitter	-	-	-	1
R1	Res.	F7GC11	-	-	-	1
S1	Res.	F7GC10	-	-	-	1

Table 3.1: Wafer inventory list for *QUDEV Mask 6 13.11.2008*: devices contained on the wafer, also see figure 3.5. Abbreviations: *MZI* stands for Mach-Zehnder Interferometer, *BS* for beam splitter, *Res.* for resonator. *3* corresponds to a chip size of 7000 $\mu m \cdot$ 6000 μm, *1* to 7000 $\mu m \cdot$ 2000 μm. See figures 3.4 a) and b) for design schematics.

3.3 Measurements

A first test measurement was carried out on device A1 using the setup introduced in section 2.2.3. The results (see figure 3.6 and 3.1) were qualitatively satisfying compared to the simulation in figure 3.1. Though, the work frequency seems to be shifted from 6.5 GHz by 500 to 600 MHz up to 7.1 GHz. Further measurements are required to determine the cause of this discrepancies which may again be due to imperfect grounding of the coplanar waveguide.
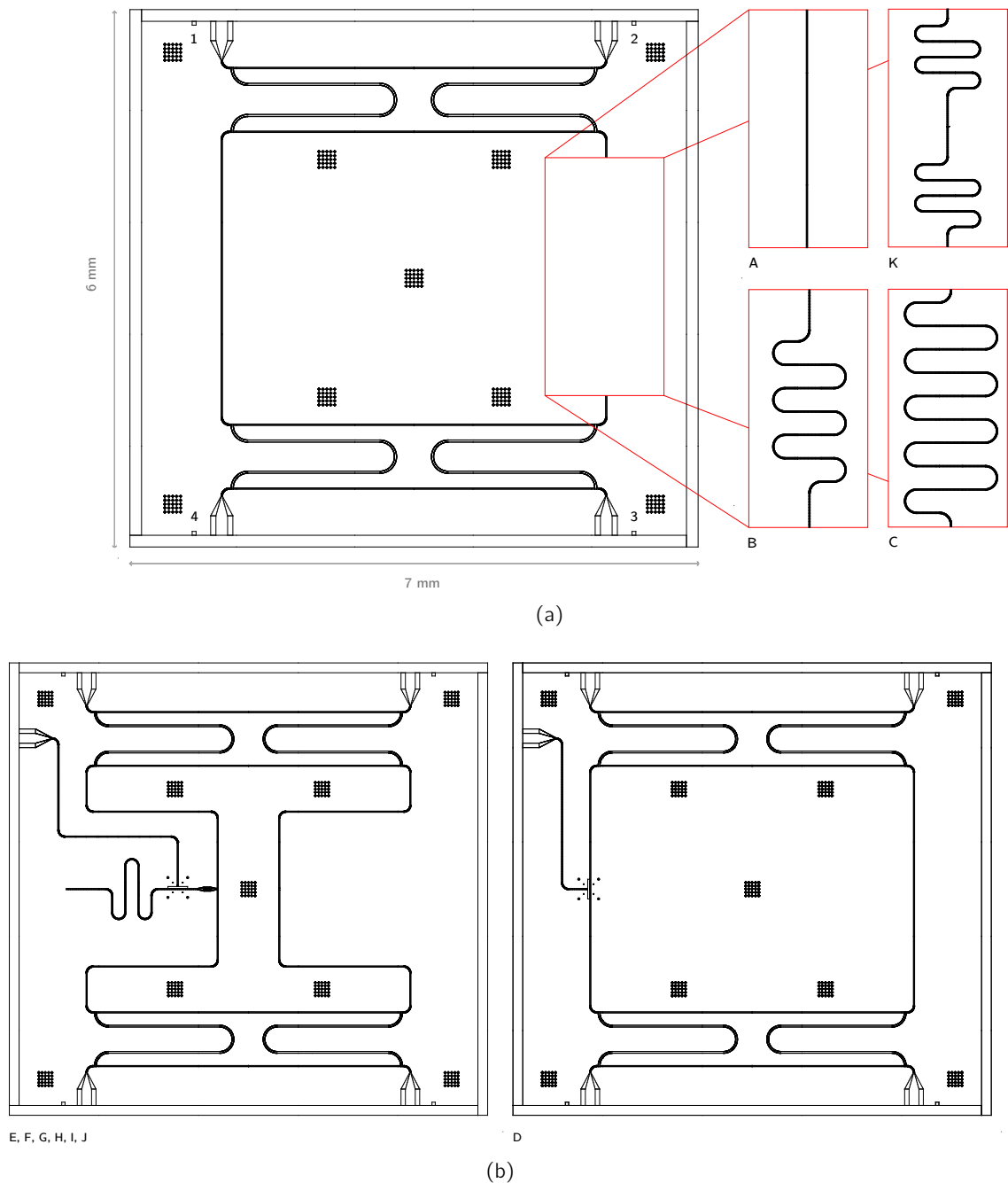
(a)

(b)

Figure 3.4: Coplanar waveguide design of Mach Zehnder Interferometers (MZI) incorporating 6.5 GHz beam splitters. Compared to figure 2.4, both beam splitter devices were rotated by 90 degrees to make the top right port (2) the terminated port. a) Captions (A, K, B, C) refer to the actual chip labeling. (A) shows a straight through MZI with zero phase shift where both arms have the same length. (B) and (C) show a 90 and 180 degree phase shift, achieved by additional transmission line lengths of $4670\,\mu m$ and $2 \cdot 4670 = 9340\,\mu m$ (as mentioned in chapter 2, equation 2.14 these lengths are the electrical lengths corresponding to 90 and 180 degrees). (K) depicts a High-Q $\lambda/2$-resonator with length of $9340\,\mu m$ and resonator gaps of $2\,\mu m$. b) $\lambda/4$ Resonator devices *E, F, G, H, I, J* (here with charge line) and straight Qubit through device *D* (right).
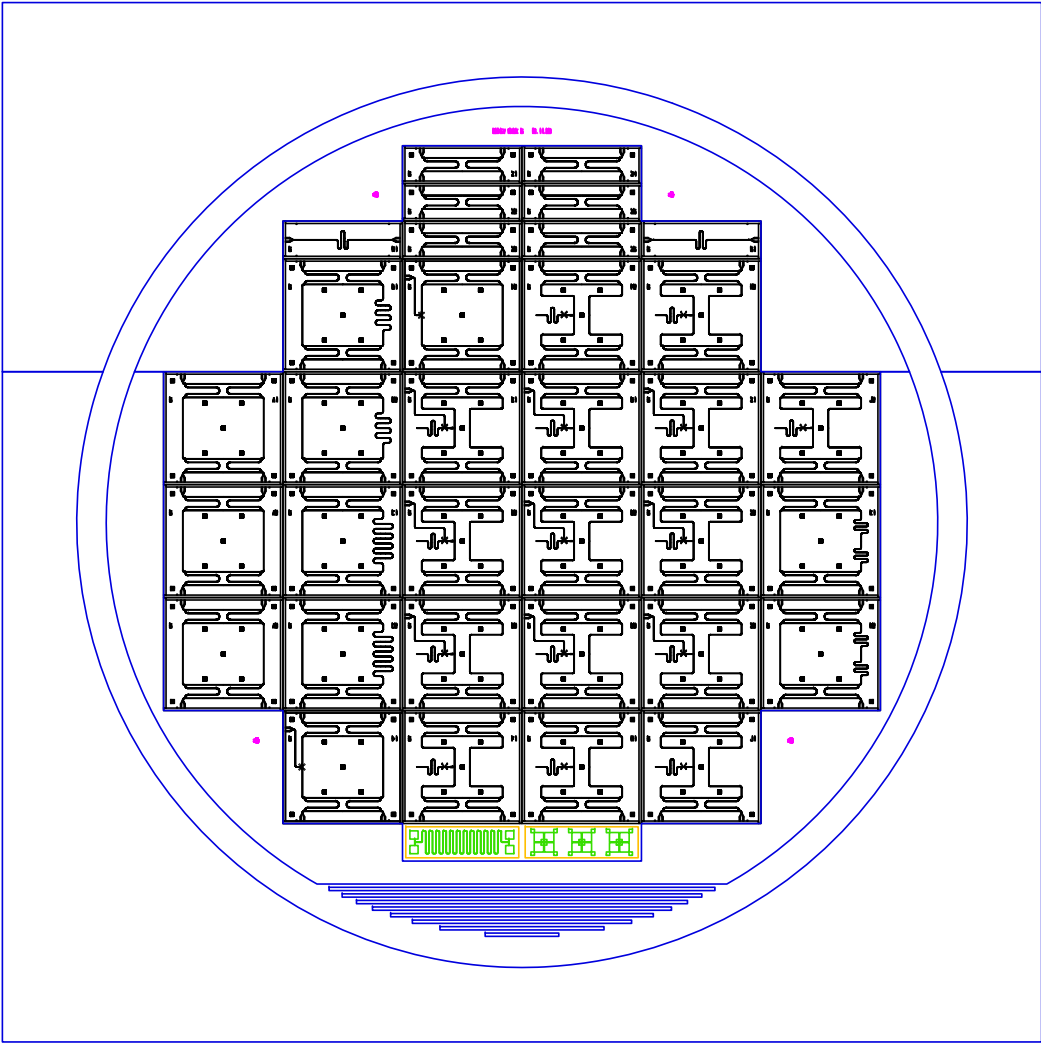
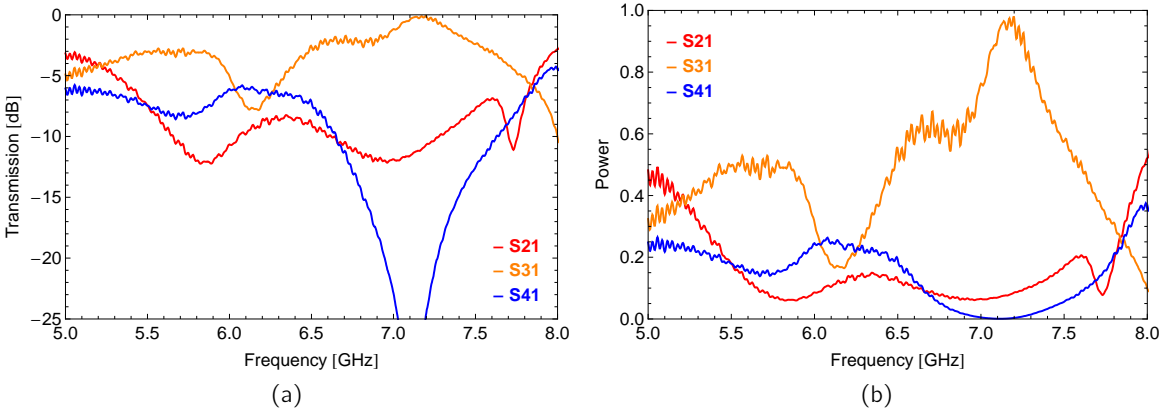Figure 3.5: Plot of *QUDEV Mask 6 13.11.2008*.

Figure 3.6: a) Measured scattering matrix parameters of a MZI A1 in dB, b) linear scaling.

4 Conclusion and Outlook

In this thesis superconducting circuit equivalents to optical beam splitters and Mach-Zehnder Interferometers were designed and corresponding devices were fabricated. Measurements of scattering matrix elements have shown that beam splitter devices qualitatively have properties that are in agreement with theoretical predictions. Bond wires were put over the coplanar waveguide transmission lines to prevent unwanted mode excitations. This improved the measurement fidelity significantly. The influence due to additional bond wires that were placed over the T-junctions can highly likely be considered as nonrelevant, however. Unwanted reflections caused by impedance mismatches in the circuits can seriously effect beam splitter performance. To eliminate these mismatches, the cabling of the dipstick was changed. The general properties of MZIs have been shown by constructing phase shift devices incorporating 90 and 180 degrees of phase shifts. Devices with qubit coupled $\lambda/4$ resonators have been designed, paving the way for new methods of qubit readout.

In future, more samples of plain Mach-Zehnder Inteferometers have to be analyzed to get statistical information about their behavior. The impact of incorporating air-bridges instead of wire bonds is needed to be shown. In addition, one needs to verify if qubit readout schemes with Mach-Zehnder Inteferometers effectively bear any advantages compared to current methods.

Acknowledgements

Bibliography

[1] Wallraff, A., Schuster, D. I., Blais, A., Frunzio, L., Huang, R. S., Majer, J., Kumar, S., Girvin, S. M., and Schoelkopf, R. J. *Nature* **431**, 162–167 (2004).

[2] Frey, T. Semester thesis, (2008).

[3] Henzen, D. Semester Thesis, (2008).

[4] Clerk, A. A., Devoret, M. H., Girvin, S. M., Marquardt, F., and Schoelkopf, R. J. arXiv:0810.4729, (2008).

[5] Pozar, D. *Microwave Engineering*. John Wiley & Sons, (1998).

[6] Simons, R. N. *Coplanar Waveguide Circuits, Components and Systems*. Wiley-Interscience, (2001).

[7] Hecht, E. *Optics*. Pearson Addison Wesley, fourth edition, (2002).

[8] Goppl, M., Fragner, A., Baur, M., Bianchetti, R., Filipp, S., Fink, J. M., Leek, P. J., Puebla, G., Steffen, L., and Wallraff, A. arXiv:0807.4094v1, (2008).

[9] Wallraff, A., Schuster, D. I., Blais, A., Frunzio, L., Majer, J., Girvin, S. M., and Schoelkopf, R. J. *Physical Review Letters* **95**, 060501 (2005).

Bibliography